Supplementary Materials:

Materials and Methods:

Mice

All mouse strains used in this study (*C57BL/6*, *St8sia4-/-*, *Ccr7-/-, Ccl19-/-*) were bred and maintained at IST Austria according to the local regulations.

Antibodies and reagents

The following antibodies and conjugates were used in this study: mouse α-CCR7-PE (4B12), rat α-mouse I-A/I-E-eFluor450 (M5/114.15.2), rat α-mouse I-A/I-E-biotin (2G9), hamster α-mouse CD11c-APC (N418), hamster α-mouse CD11c-biotin (N418), rat α-mouse B220-PE-Cy7 (RA3-6B2), rat α-mouse CD3-eFluor450 (17A2), rat α-human/mouse CD44-PE-Cy7 (IM7), Streptavidin-FITC all from eBioscience; rat α-mouse CD62L (MEL-14, BD Biosciences), rat α-mouse CD11b-BrillantViolet421 (M1/70, BD Biosciences), α-mouse CD11c-PE-Cy7 (HL3, BD Biosciences), rat α-mouse CD4-V500 (RM4-5, BD Biosciences), rat α-mouse CD103 (M290, BD Biosciences), hamster α-mouse CD69 (H1.2F3, BD Biosciences), α-mouse I-A/I-E-BrillantViolet510 (M5/114, BioLegend), rat α-mouse M1/70-PE (M1/70, Biolegend), rat α-CD8α-PerCP (53-6.7; Biolegend); rat α-CD207/Langerin-e647 (929F3.01, Dendritics); rabbit α-laminin (L9393, Sigma), rabbit α-mouse neuropilin-2 (D29A5), rabbit α-Akt (C67E7)/α-phospho-Akt (S473, D9E), rabbit α-Erk1/2 (137F5)/α-phospho-Erk1/2 (Th202/Thr204, D13.14.E) all from Cell Signaling; rabbit α-GAPDH (Abcam); mouse α-GFP antibody (2B6) was kindly provided by Stefan Schüchner and used at a final concentration of 3.5μg/ml ; goat α-mouse IgG-HRP conjugate, goat α-rabbit IgG-HRP conjugate both from Bio-Rad; donkey α-rat Alexa-Fluor488, donkey α-rat Alexa-Fluor647, Streptavidin-Cy3, all from Jackson ImmunoResearch. All commercially available antibodies and conjugates were diluted and used according to the manufacturer's recommendations.

Mouse α-polySia monoclonal antibody 735 (mab 735) and active/inactive endoneuraminidase (-GFP) were purified as described previously (*24-26*). Mab 735 was used at a final concentration of 2μg/ml.

Expression and purification of full length CCL21 (CCL21-FL 1-111), truncated CCL21 (CCL21trunc 1-79) and the CCL19/21 chimera (CCL19 1-77-CCL21 78-111)

The proteins were expressed and purified using a procedure adapted from Lu *et al*. (*27*). Codon optimized DNA coding for the desired fusion protein SMT3-CCL21 1-111 or SMT3-CCL21 1-79 were cloned into the BamHI or HindIII sites of pQE30 while SMT3-CCL19 1-77-CCL21 78-111 was cloned into the same sites in pET28a. All plasmids were sequence verified. Each expression plasmid were individually transformed into BL21 [DE3] *E. coli* (pET28A- SMT3-CCL19 1-77-CCL21 78-111) or BL21 [pREP4] *E.coli* (pQE30-SMT3-CCL21 1-111, pQE30-SMT3-CCL21 1-79).

One-liter cultures were grown at 37˚C in either lysogeny broth or [U-^{15}N] or [U-^{15}N/^{13}C] M9 minimal media to an optical density at 600nm of 0.5-0.7 and then induced with 1mM isopropyl-β-D-thiogalactopyranoside for five hours. Cell pellets were collected by centrifugation and stored at -20˚C. Cells were resuspended in 10mL of buffer A (50mM sodium phosphate, 300mM NaCl, 10mM imidazole, pH 8.0) containing 1mM phenylmethylsulfonyl fluoride (PMSF) and 0.1% (v/v) 2-mercaptoethanol. Resuspended cells were lysed by sonication and the lysate was centrifuged at 15,000 × g for 15 minutes. All the proteins expressed insolubly as an inclusion body. The inclusion bodies were separately dissolved in 10mL of buffer AD (50mM sodium phosphate, 300mM NaCl, 10mM imidazole and 6M guanidine hydrochloride, 0.1% (v/v) 2-mercaptoethanol, pH 8.0), clarified by centrifugation at 15,000 × g for 15 minutes and batch loaded onto 2mL of His60 nickel resins for thirty minutes. The columns were washed with 40mL of buffer AD and eluted with 30mL of buffer BD (100mM sodium acetate, 300mM NaCl, 10mM imidazole, and 6M guanidine HCl, pH 4.5). Elutions for the His_6-SMT3-CCL19/21, His_6-SMT3-CCL21 (1-111), and His_6-SMT3-CCL21 (1-79) fusions were dialyzed 4˚C with stirring against 4L of 0.3% acetic acid overnight and then against 4L of refolding buffer (20mM Tris, pH 8.0). After 15-20 hours, 400μg of His_6-Ulp1 (ubiquitin like protease-1) was added and left for additional 15-20 hours.

After clarification by centrifugation at 4,000 × g for 15 minutes, the digestions were separately loaded onto SP HP HiTrap™ 1mL columns at a flow rate of 2.5mL/min. The columns were washed with 15mL of wash buffer (100mM Tris, 25mM NaCl, pH 8.0) to remove His_6-SUMO and His_6-Ulp1. The chemokines were eluted with 15mL of elution buffer (100mM Tris, 2M NaCl, pH 8.0). CCL19/21 (chimera), CCL21 1-111 (CCL21-FL), and CCL21 1-79 (CCL21trunc) were further purified using reverse phase HPLC (0.1% aqueous trifluoroacetic acid buffer with a CH_3CN gradient from 21 to 42% (v/v) over 30 minutes). MALDI-TOF mass spectrometry was used (Applied Biosystems Voyager 6004) to confirm molecular weight.

Immunohistology

LNs were fixed overnight in 0.05M phosphate buffer, pH 7.4 containing 2mg/ml $NaIO_4$, 0.1mM L-lysine and 1% paraformaldehyde (all from Sigma) and dehydrated in consecutive sucrose gradients (10, 20 and 30% in 0.05M phosphate buffer) to preserve LN structures. Organs were frozen in O.C.T and cut into 10μm cryosections. Sections were air-dried before rehydrating in TBS+1% Tween (Sigma) and blocking in 1% BSA (Sigma). Antibody staining was carried out according to the manufacturer's dilution recommendations. Slides were analyzed with an upright Zeiss LSM700 confocal microscope equipped with a Plan-Apochromat 10x/0.45 objective (Zeiss). For analysis of Langerin signal intensities the background below twice the overall mean intensity was subtracted and the remaining intensity, above the threshold, normalized by the overall intensity. In this way only significant contributions above the mean intensity are considered while compensating for the varying size and brightness level of the image.

Flow Cytometry

LNs and spleens were treated with collagenase D (Roche) or II (Gibco, 0.5μg/ml) for

20 minutes at 37°C and digestion stopped with 10mM EDTA. LNs and spleen were mechanically crushed to isolate immune cells and erythrocytes of spleen were lysed in red blood cell (RBC) buffer containing ammonium chloride (1.7M), potassium hydrogen carbonate (100mM), and EDTA (1mM). Before staining, 1-2x10^6 cells were incubated for 15 min at room temperature with blocking buffer (RPMI, 10% FCS, 5mM EDTA) containing 5mg/ml α-CD16/CD32 (2.4G2, BD Biosciences). For surface staining, cells were incubated for 30 min on ice with conjugated monoclonal antibodies (mAbs) diluted at the recommended concentration in blocking buffer. iEndoN-GFP was used at a final concentration of 0.6mg/ml. Flow cytometry analysis was performed on a FACS CANTO II flow cytometer (BD Biosciences). For phenotypic analysis of Langerin$^+$ cells, after surface staining and fixation in 1% paraformaldehyde, cells were permeabilized with 0.5% saponin and intracellular staining was performed with α-mouse Langerin antibody for 45 minutes.

In vivo lymphocyte homing assay

Naïve lymphocytes were isolated from LNs and spleen (after RBC lysis) of *St8sia4*-/- and control mice and labeled with 10μM 5-(and-6-) Carboxytetramethylrhodamine, Succinimidyl Ester (TAMRA) or 5μM Carboxyfluorescein Succinimidyl Ester (CFSE; both Molecular Probes, Life Technologies) in PBS, 0.01% BSA. Labeling was stopped by adding 5 volumes of full media (R10; RPMI 1640 supplemented with 10% FBS, L-Glutamin, β-ME and Penicillin/Streptomycin, all from Invitrogen). 15-20x10^6 labeled lymphocytes were injected intravenously in PBS into *St8sia4*-/- and control recipient mice. Three hours after injection, mice were sacrificed and lymphocytes isolated from LNs and spleen to recover transferred cells. The percentage of fluorescent cells recruited to each lymph node was determined by flow cytometry.

Generation of bone marrow derived dendritic cells and footpad injections

Bone marrow-derived dendritic cells (BMDCs) were generated from flushed bone marrow suspension as previously described (*28*). Cells were grown in R10 medium supplemented with 20% GM-CSF hybridoma supernatant for seven to nine days before stimulation with 200ng/mL LPS (Sigma-Aldrich; *E.Coli* 0127:B8) over night. Mature BMDCs were labeled with 10μM 5-(and-6-) Carboxytetramethylrhodamine, Succinimidyl Ester (TAMRA) or 5μM Carboxyfluorescein Succinimidyl Ester (CFSE; both Molecular Probes, Life Technologies), respectively. Labeling was stopped by adding 5 volumes of R10 media. A total amount of 5x10^6 cells in 50μl PBS (2.5x10^6 cells/color) were injected into the hind footpad of recipient mice, which were sacrificed 48 hours later and popliteal LNs analyzed by flow cytometry. For phenotypic analysis of maturated DC *in vivo*, 10μg of LPS diluted in 50μl of PBS were injected into one food pad.

FITC painting

For experiments involving the tracking of skin DC into the lymph node after skin inflammation, *St8sia4*-/- and control mice were anesthetized with isofluorane and each side of the ear was painted with 25μl of 2% FITC solution prepared in dibutylphtalate/acetone (1/1 vol/vol; Sigma-Aldrich). Three days later, mice were sacrificed and a lymph node cell suspension was generated from the pool of draining

cervical LNs. To calculate the total number of recruited skin Langerin^{+} DCs into the lymph nodes, the total number of lymph node cells, was multiplied by the percentage of CD11c^{+}MHCII^{high}Langerin^{+}FITC^{+} cells measured by flow cytometry.

Ex vivo crawl-out migration assay and immunostaining of mouse ear sheets

Mouse ear sheets were prepared as previously demonstrated (*17*) with the following modifications: ventral ear sheets were incubated up-side-down in R10 medium for 48 hours and subsequently fixed with 1% paraformaldehyde over night. Ear sheets were permeabilized with 0.2% Triton/PBS for 15 minutes and blocked with 1% BSA (PAA Laboratories) for one hour. Staining of lymphatic vessels and mature DCs was carried out using α-LYVE-1 and α-MHCII-biotin primary antibodies diluted in 1% BSA and secondary antibodies conjugated to FITC and Streptavidin-Cy3, respectively.

For end point analysis of crawl-in assays, ventral ear sheets were mounted and immunostained in custom-made chambers using LYVE-1 primary- and Alexa647-conjugated secondary antibodies as described above. A total of $1x10^{6}$ labeled BMDCs was added in R10 medium on top of the ear sheets and incubated for 15 minutes at 37°C to allow entering of cells into the dermis. Ear sheets were rinsed twice with R10 medium and incubated at 37°C for two hours before fixing with 1% paraformaldehyde. Confocal images of ear explants were acquired using an upright Zeiss LSM700 confocal microscope equipped with a Plan-Apochromat 20x/0.8 objective (Zeiss). Maximum intensity projections were analyzed with Fiji software to reconstitute lymphatic vessel structures according to LYVE-1 staining. DC location was estimated manually for at least five different regions per ear sheet and at least three different mice per genotype.

Intralymphatic injections

C57BL/6 mice were housed and bred in a pathogen-free animal facility. Mice were anesthetized by intraperitoneal injection of 20mg/kg xylazine and 100mg/kg ketamine. After leg-depilation with cream, a skin incision was made on the dorsal side of the lower hind leg and the main lymphatic vessel draining the footpad area to the popliteal lymph node was exposed by microsurgery. A glass capillary (3 in., 1.2mm/0.68mm OD/ID; WPI) was pulled with a micropipette puller (Model P-97; Sutter instrument CO), broken and grounded with a micropipette grinder (MicroData Instrument, Inc). BMDCs were labeled for 15 min at 37°C with 10μM TAMRA in PBS, 0.01% BSA and the microcapillary was filled with 5μl cell suspension (in PBS) using to a PLI-100A microinjector (Harvard Apparatus). A micromanipulator (Kleindiek Nanotechnik) was used for the stabilization of the capillary during injection. A pressure of approximately 5kPa in 120s pulses was used for the delivery of cells, avoiding injection of air. At all times during surgery, exposed tissues were kept moist with sterile PBS and observed with Leica M125 stereomicroscope. Incisions were closed with tissue adhesive (3M Vetbond) at the end of surgery. The draining popliteal LN was harvested 10h later, fixed overnight in PLP fixative buffer (0.05M phosphate buffer, 0.1M L-lysine, pH 7.4, 2 mg/ml NaIO4, 10 mg/ml paraformaldehyde), and dehydrated in consecutive sucrose gradients (10, 20, and 30% in phosphate buffer). Tissues were snap frozen in Tissue-Tek. 6μm frozen sections were stained with rabbit α-laminin Ab (Sigma- Aldrich) and secondary α-rabbit Alexa 647 Ab to visualize LN structures and localize injected BMDCs. Representative images were analyzed using IMARIS imaging software.

Based on the laminin staining, surface corresponding to the outside border of the cortical sinus was selected manually. A distance transformation was performed outside this new defined surface, yielding a new (distance-) channel with intensity values directly corresponding to the distance of the nearest edge of the isosurface. TAMRA-labeled cells were represented as dots and distance-channel intensities were used for quantifying the average migratory distance from the LN's edge.

Chemotaxis assays

In vitro 3D dendritic cell migration assays have been carried out as previously described (*29*). Briefly, 3-4x10^5 cells were suspended in a medium:collagen mixture (PureCol bovine collagen, (INAMED) in 1× minimum essential medium eagle (MEM, Invitrogen)) and 0.4% sodium bicarbonate (Sigma) at a volume ratio of 1:2 yielding in a final collagen concentration of 1.6mg/ml. Collagen gel mixtures were casted into custom-made migration chambers and incubated for 45 minutes at 37°C to allow polymerization of the gel. Individual chemokines were suspended in R10 medium to a final concentration of 0.33µM and placed on top of the gel. DC migration was followed by time-lapse video microscopy and cells tracked either manually by using the 'Manuel tracking- and chemotaxis tool' plug-in provided by Fiji or automated by an in-house generated algorithm.

Automated cell tracking

Average migration speed of all cells was calculated for each time point using a custom made script, determining lateral displacements that optimizes its overlap with the previous frame. Migration speed was calculated from the optimal y-displacement in pixels, divided by the time between two consecutive frames.

Generation and transfection of CCR7-GFP glycosylation mutants

Mouse CCR7-GFP expression plasmid (pcDNA3.1-) was a gift of Daniel Legler and the plasmid encoding full length hamster ST8Sia IV was generated as described (*30*). Individual putative CCR7 glycosylation sites were mutated to alanine by using the site directed mutagenesis kit (Stratagene) according to the manufacturer's instructions. HEK293 cells were grown in DMEM (Invitrogen) supplemented with 10%FBS and transfected using Lipofectamine (Invitrogen) at 80% confluence.

Protein extraction, Immunoprecipitation and Western blotting

To identify polysialylated proteins in mature DCs, 1x10^6 cells were lysed in 500µl RIPA buffer (Cell Signaling) containing 50µl/ml protease inhibitor cocktail (Roche) and subsequently incubated with inactive EndoN-coupled to MyOne® tosylactivated Dynabeads (Invitrogen) at +4°C under constant rotation. Coupling of Dynabeads was carried out according to the manufacturer's recommendations. Proteins were eluted with 100mM Glycine, pH 2.0 at room temperature and subjected to mass spectrometric analysis. For *in vitro* reconstitution of CCR7 polysialylation, transfected HEK293 cells of one well of a 6-well plate were lysed in 60µl RIPA buffer containing 50µl/ml protease inhibitor cocktail. Polysialylated proteins were immunoprecipitated and eluted as described above. 6µl of cell lysate was retained as input. To remove polySia from

N- and O-glycans whole cell lysates were incubated with active EndoN at a final concentration of 1.5µg/ml for two hours at 37°C.

Proteins were separated by SDS-PAGE under reducing conditions and transferred to a polyvinylidene difluoride membrane (Invitrogen). Primary antibodies were used according to the recommended dilutions and detected by peroxidase-conjugated α-mouse IgG or α-rabbit IgG antibodies. Detection of proteins was performed by enhanced chemiluminescence (ECL) detection using a VersaDoc imaging system (Biorad).

MS-based protein identification

The nano HPLC system used was an UltiMate 3000 HPLC RSLC nano system (Thermo Fisher Scientific, Amsterdam, Netherlands) coupled to a Q Exactive mass spectrometer (Thermo Fisher Scientific, Bremen, Germany), equipped with a Proxeon nanospray source (Thermo Fisher Scientific, Odense, Denmark). Peptides were loaded onto a trap column (Thermo Fisher Scientific, Amsterdam, Netherlands, PepMap C18, 5 mm × 300 µm ID, 5 µm particles, 100 Å pore size) at a flow rate of 25µL min^{-1} using 0.1% TFA as mobile phase. After 10 min, the trap column was switched in line with the analytical column (Thermo Fisher Scientific, Amsterdam, Netherlands, PepMap C18, 500 mm × 75 µm ID, 2 µm, 100 Å). Peptides were eluted using a flow rate of 230 nl min^{-1}, and a binary 2h gradient, respectively 165 min. The gradient starts with the mobile phases: 98% A (water/formic acid, 99.9/0.1, v/v) and 2%B (water/acetonitrile/formic acid, 19.92/80/0.08, v/v/v) increases to 35%B over the next 120 min, followed by a gradient in 5 min to 90%B, stays there for five min and decreases in 5 min back to the gradient 98%A and 2%B for equilibration at 30°C.

The Q Exactive mass spectrometer was operated in data-dependent mode, using a full scan (m/z range 350-2000, nominal resolution of 70 000, target value 1E6) followed by MS/MS scans of the 12 most abundant ions. MS/MS spectra were acquired using normalized collision energy 30%, isolation width of two and the target value was set to 1E5. Precursor ions selected for fragmentation (charge state two and higher) were put on a dynamic exclusion list for 30 seconds. Additionally, the underfill ratio was set to 20% resulting in an intensity threshold of 5E4. The peptide match feature and the exclude isotopes feature were enabled.

Data Analysis

For peptide identification, the RAW-files were loaded into Proteome Discoverer (version 1.4.0.288, Thermo Scientific). All hereby created MS/MS spectra were searched using MS Amanda against the human swissprot protein sequence database (from 2014-07-06; 16678 sequences, 9357021 residues). The following search parameters were used: β-methylthiolation on cysteine was set as a fixed modification, oxidation on methionine was set as variable modification. Monoisotopic masses were searched within unrestricted protein masses for tryptic peptides. The peptide mass tolerance was set to ±10 ppm and the fragment mass tolerance to ±20 ppm. The maximal number of missed cleavages was set to 2. The result was filtered to 1% FDR using Percolator algorithm integrated in Thermo Proteome Discoverer. All non-mouse proteins were excluded from the list. Protein Areas are calculated as average of the three highest peptide areas, also integrated in Thermo Proteome Discoverer.

Signaling assays

Mature DCs were stimulated with 20ng/ml chemokine for the indicated time points and subsequently lysed in RIPA buffer containing 50µl/ml protease and phosphatase inhibitor cocktail (both from Roche) at +4°C. Protein lysates were separated by SDS-PAGE, followed by immunoblotting and detection of the respective (phospho)- proteins as described above.

Protein NMR

All NMR experiments were performed at 25˚C at the Medical College of Wisconsin NMR facility on either a Bruker 600 or 500 MHz spectrometer equipped with a triple resonance cryoprobe. All NMR samples contained the same NMR buffer (25mM deuterated MES, 10% D_2O, 0.02% NaN_3, pH 5.9). Spectra of [U-^{15}N] CCL21trunc (residues 1-79) and full length [U-^{15}N] CCL21 (residues 1-111) were collected at a protein concentration of 200µM. Titrations of [U-^{15}N] CCL21trunc (residues1-79) and full length [U-^{15}N] CCL21 (residues 1-111) with incremental additions of polysialic acid (DP9) were monitored by ^{15}N-^{1}H HSQC spectra. Backbone amide chemical shift perturbations were computed as $[(5\Delta\delta_H)^2 + (\Delta\delta_N)^2]^{0.5}$ where $\Delta\delta_H$ and $\Delta\delta_N$ are the change in backbone amide ^{1}H and ^{15}N chemical shift, respectively. Dissociation constants were determined using the equation

$$\Delta\delta = \Delta\delta_{\max} \times \frac{(K_d + [\mathrm{CCL21}] + x) - \sqrt{(K_d + [\mathrm{CCL21}] + x)^2 - 4[\mathrm{CCL21}]x}}{2[\mathrm{CCL21}]}$$

where $\Delta\delta$ is the chemical shift perturbation, $\Delta\delta_{max}$ is the maximum chemical shift perturbation at 100% bound CCL21, K_d is the dissociation constant, and x is the polySia (DP9) concentration. PolySia (DP9) was produced as previously described (*31*, *32*).

Statistical analysis

Results are expressed as mean ±SD with n numbers indicated for each experiment. Differences between two groups were examined by two-tailed unpaired student's t-tests. For intralymphatic injections differences were examined by two-tailed paired student's t-test. *P<0.05, **P<0.01 and ***P<0.001.

Results and Legends of Supplementary Figures

Fig. S1. PolySia on dendritic cells is required for regular lymph node homeostasis

Results

*In order to identify polySia on different immune cells we prepared cell suspensions from LNs of St8sia4-/- and control mice and analyzed them by flow cytometry. We could not detect polySia on B and T cells (**Figure S1A**). Accordingly, lymphocyte trafficking was unaffected in St8sia4-deficient and control mice revealing that polySia is dispensable for T cell homing (**Figure S1B**). Further classification of dendritic cell subsets revealed polySia expression on the surface of migratory MHCII^{high}/Langerin^{+} DCs and on conventional CD8^{+} DCs (**Figure S1C**) as well as on bone marrow derived DCs (**Figure S1D**)..*

Legend

(A) Flow cytometry of lymphocytes isolated from either PLNs or spleen of *St8sia4-/-* and control mice and analyzed for cell surface polySia levels. B and T cells were specified according to B220^{+} and CD3^{+} staining and analyzed for cell surface polySia levels. PolySia staining has been carried out with inactive EndoN-GFP.

(B) *In vivo* short-term homing of *St8sia4-/-* and control lymphocytes in wild type and polySia-deficient recipient mice. *St8sia4-/-* and control lymphocytes were isolated from PLNs and spleen and labeled with 10µM TAMRA or 5µM CFSE, respectively. PLNs and spleens of recipient mice were removed three hours after injection and analyzed by flow cytometry. Graphs depict average percentage of fluorescent cells within SLOs of at least 5 different mice per genotype ±SD. Differences between the two groups were examined by two-tailed unpaired student's t-test.

(C) Specification of DC subsets positive for cell surface polySia under steady state conditions. DC sub-populations were classified according to CD11b^{+}, CD8^{+} and Langerin^{+} staining.

(**D**) (left) Immunodetection of total polySia levels in whole cell lysates of immature CD11c^{+} MHCII^{low} (iDCs) and mature CD11c^{+} MHCII^{high} (mDCs) BMDCs. (right) Cell surface polySia levels in immature and mature BMDCs.

Fig. S2. Non-polysialylated CCR7 shows impaired signaling towards CCL21

Results

*Upon chemokine binding, CCR7-mediated G protein activation triggers distinct intracellular signaling cascades involving MAP kinases as well as the PI3K/Akt pathway (33). To dissect the contribution of these signaling pathways to polySia-mediated chemotaxis we stimulated LPS-treated St8sia4-/- and control BMDCs with either CCL19 or CCL21 and compared the levels of phosphorylated effector kinases. CCL19 stimulation led to a transient phosphorylation of Akt and Erk in both cell types with strongest signals 2-5 min after stimulation (**Figure S2**). However, phosphorylation levels of both kinases in St8sia4-/- DCs were significantly lower after CCL21 stimulation, indicating that in the absence of polySia, CCR7 does not trigger intracellular signaling cascades upon CCL21 stimulation. These results are consistent with the observed migration defect of St8sia4-/- DCs.*

Legend

BMDCs from *St8sia4-/-* and control mice were maturated with LPS over night and adjusted to equal cell numbers the next day. Cells were stimulated with 20ng/ml CCL19 (left panel) or CCL21 (right panel) for the indicated time points and immediately harvested and lysed on ice. Membranes were probed with specific phospho-kinase antibodies as well as total kinase levels. Shown are representative immunoblots of three independent experiments.

Fig. S3. Polysialylation affects CCL21 sensing in peripheral tissues

Legend

(A) Schematic representation of experimental setup and chemokine guidance of *in vivo* DC migration. In contrast to footpad injections, fluorescently labeled BMDCs were injected directly within the afferent lymphatic vessel of *Ccl19*-/- recipient mice. Draining popliteal LNs were analyzed by immunohistology 10 hours later.

(B) (left) z-stack projection of split ear sheets stained against LYVE1 (green) and MHCII (red). Respective genotypes are indicated above. **(right)** Quantification of DCs inside lymphatic vessels. Bars represent average values ±SD of five different fields per ear of three different animals. Differences between the two groups were examined by two-tailed unpaired student's t-test. Scale bar: 100µm.

(C) (left) Immunoblotting of polySia in activated *St8sia4*-/- and activated control T cells in comparison to mature dendritic cells (mDCs). **(right)** Activated *St8sia4*-/- and control T cells were embedded within 3D collagen I matrices and exposed to soluble gradients of CCL19 and CCL21. Average y-directed velocities ±SD of 6 experiments with cells from 3 different mice are shown over time.

Fig. S4. Migration of *Nrp2*-deficient dendritic cells and polysialylation of CCR7 on mature dendritic cells

Results

Migration of Nrp2-deficient dendritic cells

Neuropilin-2 (NRP-2) is the only known potential carrier of polySia, which is abundantly expressed on DCs and as such has been implicated in CCL21 responses (*7-9*, *23*). *To address whether loss of polysialylated NRP-2 is responsible for the DC-specific migration defect in St8sia4-/- animals we used ear explants and BMDCs from Nrp-2-deficient mice* (*34*) *and determined migration as previously described* ((*17*); ***Figure S4A***). *BMDCs from Nrp-2-/- and control mice both entered the lymphatic vessels equally well when incubated on wildtype ear explants suggesting that NRP-2 is dispensable for DC migration in vivo. Accordingly, analysis of gradient-directed velocities, as described in the main text, did not reveal a difference between Nrp-2-/- and control BMDC migration towards CCL19 or CCL21 (**Figure S4B**). These data demonstrate that polysialylated NRP-2 is dispensable for chemokine sensing of murine DCs. Furthermore, so far unidentified polySia carrier must be responsible for the observed migration defect in St8sia4-deficient mice.*

Polysialylation of CCR7 on mature dendritic cells

*To identify additional polySia carriers, proteins from whole cell lysates of Nrp-2-/- BMDCs were immunoprecipitated using inactive EndoN covalently coupled to magnetic beads. The protein fraction was analyzed by mass spectrometry leading to four so far unknown polysialylated proteins with CCR7 as the sole cell surface protein (**Figure S4C**). To confirm modification of CCR7, we reconstituted CCR7 polysialylation in HEK293 cells. Due to the lack of specific antibodies, we expressed CCR7-green fluorescent protein (GFP) fusion protein together with the polysialyltransferase ST8SiaIV in HEK293 cells. Immunoprecipitation of CCR7-GFP and subsequent separation of whole cell lysates by SDS-PAGE followed by*

*immunoblotting revealed a dispersed signal between 220 and 120kDa (**Figure 3A**). In addition to glycosylation, CCR7 was shown to be constitutively ubiquitylated on several lysine residues in HEK293 cells (35) explaining the highly dispersed signal of CCR7-GFP at high molecular weight.*

*Glycans can be attached to the free amide nitrogen of an asparagine residue placed in the sequence Asn-X-Ser/Thr (N-linked glycosylation) or to the hydroxyl oxygen of serine and threonine residues (O-linked glycosylation). Since polySia is attached to the extracellular part of the receptor, we searched for putative glycosylation sites within the N-terminus and the three extracellular loops of CCR7, a heptahelical transmembrane GPCR, and found two matching consensus sequences allowing N-glycosylation (Asn36 and Asn292). To confirm polysialylation of N-glycans at these sites, Asn36 and Asn292 were mutated to alanine by site-specific mutagenesis leading to three different glycosylation-mutants (**Figure S4D**, left panel). Whole cell lysates and immunoprecipitates from N-glycosylation deficient mutants of CCR7-GFP showed a shift in mobility towards lower molecular weight indicating that CCR7 is indeed N-glycosylated (**Figure S4D**, right panel). Yet, pull-down of CCR7-GFP and immunodetection with mAb 735 revealed polysialylation of CCR7 even for the double mutant ($CCR7^{N36A,N292A}$) indicating additional attachment sites of polySia chains presumably to O-linked glycans.*

*To distinguish between N- and O-linked polysialylation of CCR7, we treated HEK293 cells with the glycosylation inhibitors kifunensine and α-benzyl GalNAc. Kifunensine inhibits N-glycosylation by preventing α-mannosidase I from trimming mannose residues from precursor glycoproteins. α-benzyl GalNAc is a structural analogue of GalNAc-Ser/Thr and blocks O-glycan synthesis as it is used as surrogate substrate or decoy by glycosyltransferases involved in the extension of GalNAc-Ser/Thr sites. Treatment of HEK cells with either of the two inhibitors did not interfere with cell growth and cell surface CCR7-GFP expression (data not shown). However, treatment with both inhibitors strongly interfered with cell growth and led to dettachment of cells. Consequently transfection rates with CCR7-GFP were very poor (data not shown). PolySia levels from whole cell lysates were strongly reduced after inhibition of O-linked glycosylation (**Figure S4E**, right panel, input). Immunoprecipitation of CCR7-GFP and subsequent immunodetection of polySia still showed polysialylation of CCR7 after inhibition of either N- or O-linked glycosylation (**Figure S4E**, right panel, IP) verifying polysialylation of CCR7 on N- and O-glycosylation sites. Alltogether these results establish CCR7 as a highly glycosylated protein with terminal polySia residues attached to N- and O-linked glycans.*

Legend

(A) (right) z-stack projection of wild type split ear sheets incubated with eFluor630-labeled *Nrp-2-/-* (green) and TAMRA-labeled control (red) BMDCs. Ears were stained against LYVE1 (Alexa488; grey) to visualize lymphatic vessels. **(left)** Quantification of cells inside lymphatic vessels. Bars indicate average values ±SD of five different fields per view of three independent experiments. Scale bar: 100μm.

(B) Mature *Nrp-2* and control BMDCs were embedded within 3D collagen I matrices and exposed to soluble gradients of CCL19 and CCL21. Average y-directed velocities ±SD of 6 experiments with cells from 3 different mice are shown over time.

(C) List of proteins containing peptides identified by mass spectrometry after pull-down of polySia with iEndoN-coupled magnetic beads in *Nrp-2-/-* BMDCs. Numbers indicate different peptides of the respective protein identified. Only the most abundant proteins with at least two peptides matching the detected sequences with >99% probability were considered.

(D) (left panel) *Ccr7-gfp* constructs. Due to the lack of specific antibodies, CCR7 was expressed as GFP-fusion protein. Putative N-glycosylation sites were mutated to alanine by site-directed mutagenesis (N36A, N292A). All *Ccr7-gfp* constructs were co-expressed together with the polysialyltransferase ST8Sia IV. (right panel) Pull-down of CCR7-GFP constructs from HEK293 cells using α-GFP-coupled magnetic beads. CCR7-GFP and polySia were detected using α-GFP and monoclonal antibody 735, respectively.

(E) Inhibition of N- and O-glycosylation in HEK293 cells co-transfected with *Ccr7-gfp* and *St8sia4* plasmids. Cells were treated with kifunensine and α-benzyl GalNAc for 4 days before pull-down of CCR7-GFP using α-GFP-coupled magnetic beads. CCR7-GFP and polySia were detected as described above.

Fig. S5. Identification of an autoinhibitory interaction site within CCL21

(A) Chemical shift differences (Δδ) between 200 μM CCL21trunc 1-79 and CCL21-FL 1-111 plotted versus CCL21 residue number to identify CCL21 residues involved in autoinhibition.

(B) CCL21-FL 1-111 chemical shift perturbations induced by a 5-fold molar excess of polySia (DP9) plotted versus CCL21 residue number. The insert shows a plot of CCL21 chemical shift perturbations for residue 66 (dots) and 70 (diamonds) upon titration with DP9. The K_d was determined using a model that takes into account ligand depletion and non-linear regression.

(C) CCL21trunc 1-79 chemical shift perturbations induced by a 5-fold molar excess of polySia (DP9) plotted versus CCL21trunc residue number. The insert shows a plot of CCL21trunc chemical shift perturbations upon titration with DP9. The K_d was determined using a model that takes into account ligand depletion and non-linear regression.

Supplementary Table

Table S1. List of all identified mouse proteins by MS Amanda including their accession number, gene name, molecular weight, sequence coverage, number of peptides, number of peptide spectrum matches (PSMs) and precursor area.

Figure S1

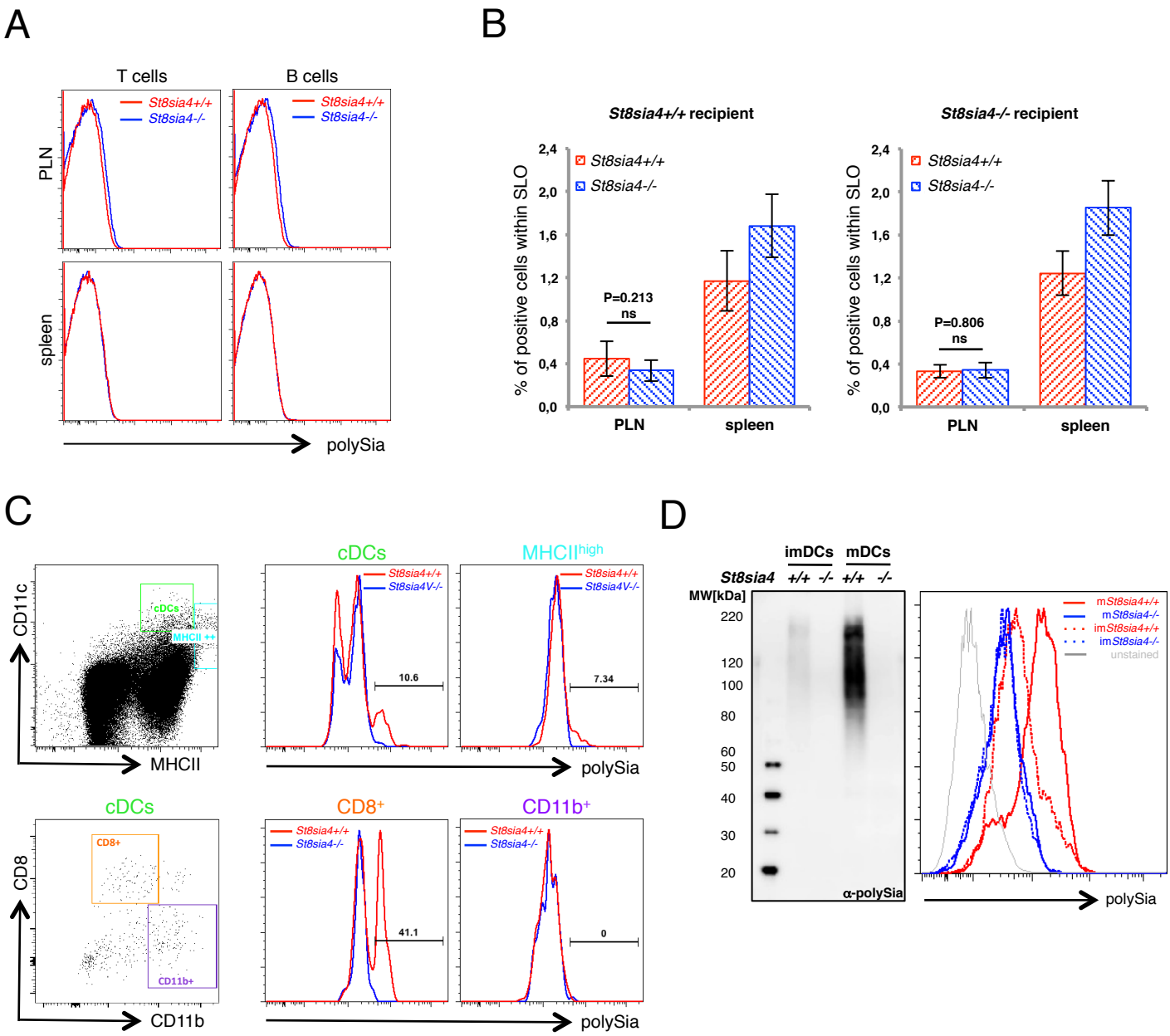
A
T cells
B cells
St8sia4+/+
St8sia4-/-
PLN
spleen
polySia
B
St8sia4+/+ recipient
St8sia4-/- recipient
% of positive cells within SLO
2,4
2,0
1,6
1,2
0,8
0,4
0,0
P=0.213
ns
P=0.806
ns
PLN
spleen
C
CD11c
MHCII
cDCs
MHCII ++
St8sia4V-/-
10.6
7.34
MHCIIhigh
CD8
CD11b
CD8+
CD11b+
41.1
0
CD8+
CD11b+
D
imDCs
mDCs
St8sia4
+/+
-/-
MW[kDa]
220
120
100
80
60
50
40
30
20
α-polySia
mSt8sia4+/+
mSt8sia4-/-
imSt8sia4+/+
imSt8sia4-/-
unstained

Figure S2

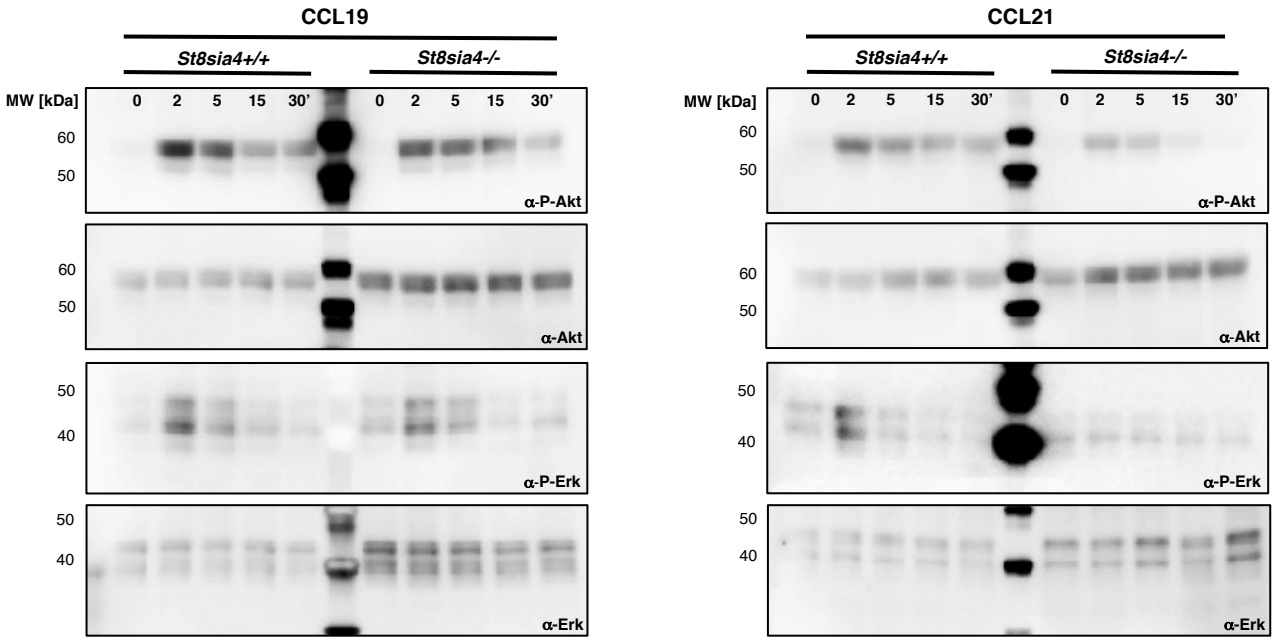
CCL19
St8sia4+/+
St8sia4-/-
MW [kDa]
0 2 5 15 30' 0 2 5 15 30'
60
50
α-P-Akt
60
50
α-Akt
50
40
α-P-Erk
50
40
α-Erk
CCL21
St8sia4+/+
St8sia4-/-
MW [kDa]
0 2 5 15 30' 0 2 5 15 30'
60
50
α-P-Akt
60
50
α-Akt
50
40
α-P-Erk
50
40
α-Erk

Figure S3

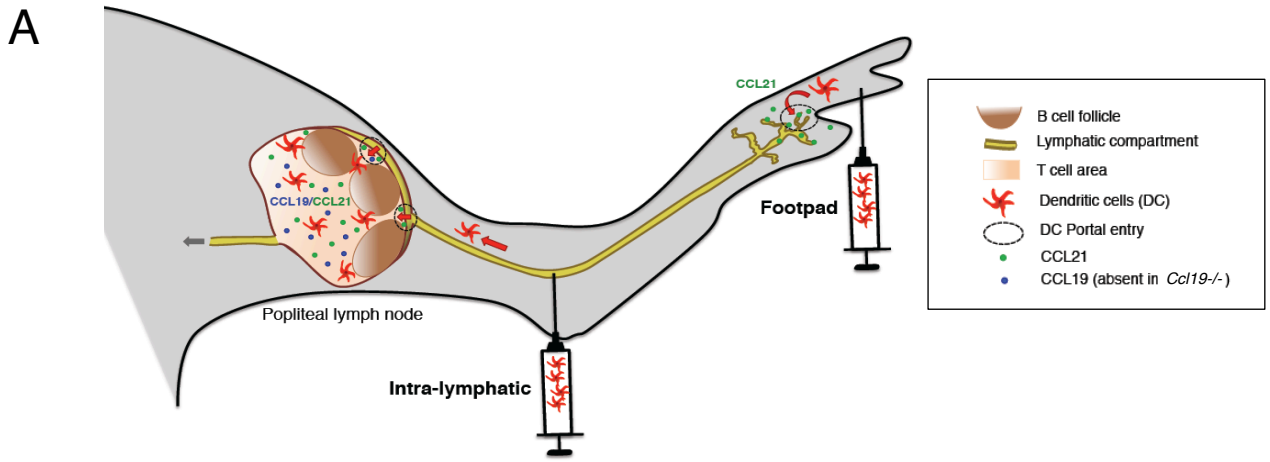
A
CCL21
CCL19/CCL21
Footpad
Popliteal lymph node
Intra-lymphatic
B cell follicle
Lymphatic compartment
T cell area
Dendritic cells (DC)
DC Portal entry
CCL21
CCL19 (absent in Ccl19-/-)

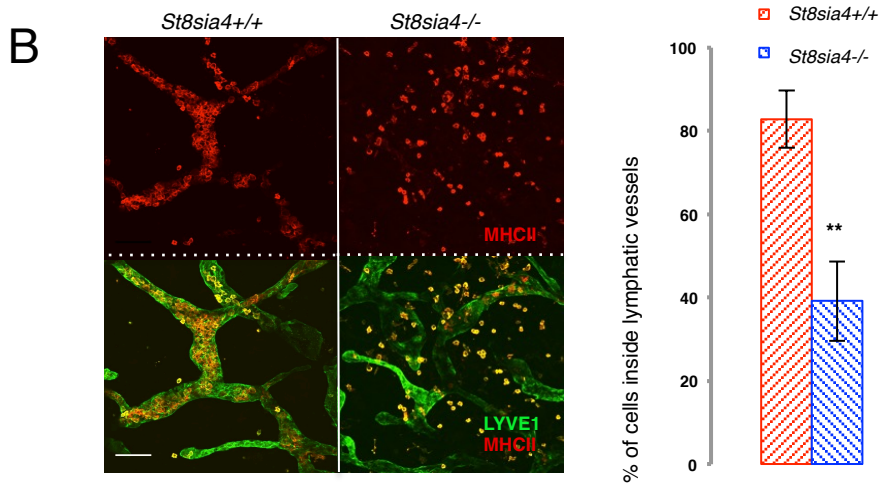
B
St8sia4+/+
St8sia4-/-
MHCII
LYVE1
MHCII
St8sia4+/+
St8sia4-/-
% of cells inside lymphatic vessels
100
80
60
40
20
0
**

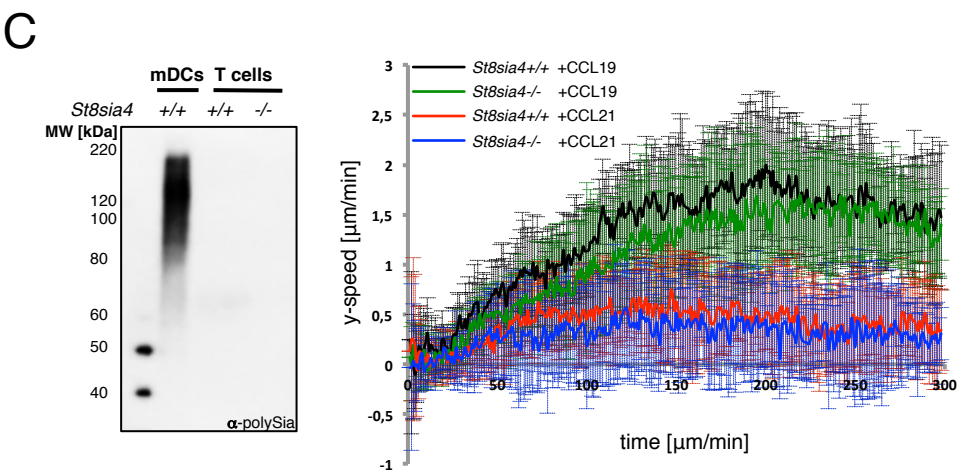
C
mDCs
T cells
St8sia4
+/+
+/+
-/-
MW [kDa]
220
120
100
80
60
50
40
α-polySia
St8sia4+/+ +CCL19
St8sia4-/- +CCL19
St8sia4+/+ +CCL21
St8sia4-/- +CCL21
y-speed [µm/min]
time [µm/min]

Figure S4

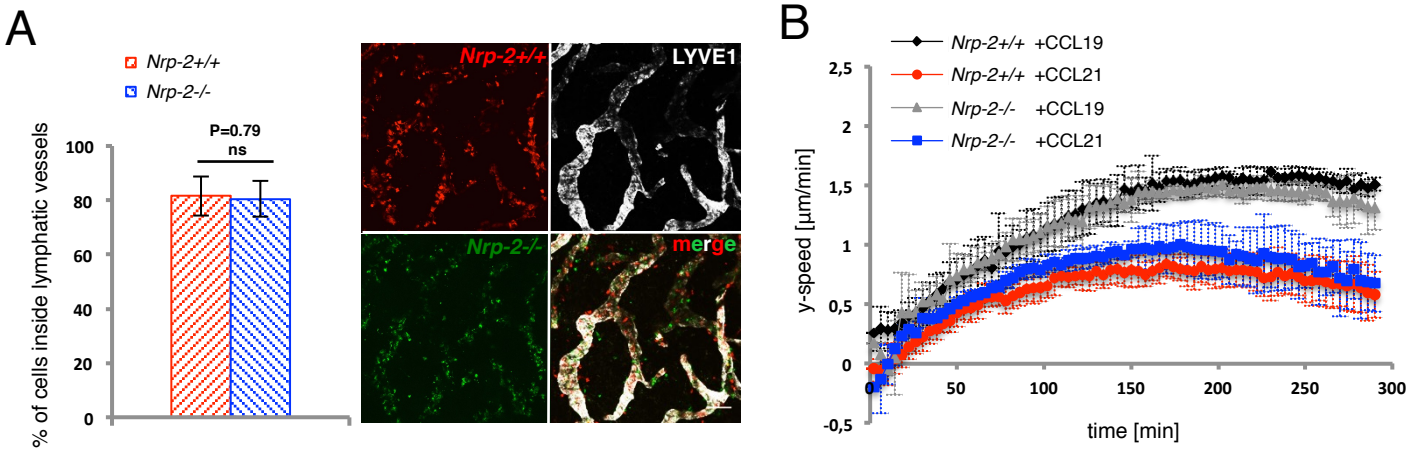

C

IP	*Ccr7-/-*	*St8sia4-/-*	*Nrp-2-/-*
Golgi apparatus protein Glg1	18		20
EH domain containing protein Ehd1			13
Cathepsin G	2		4
CCR7			**3**
Neuropilin-2	2		

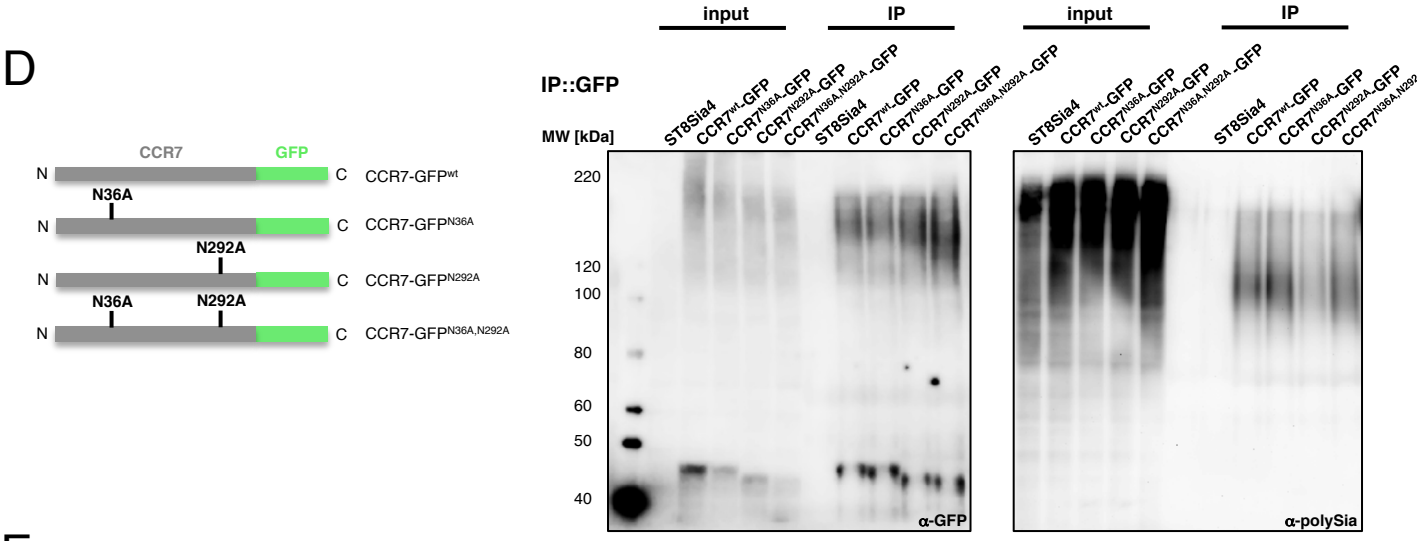

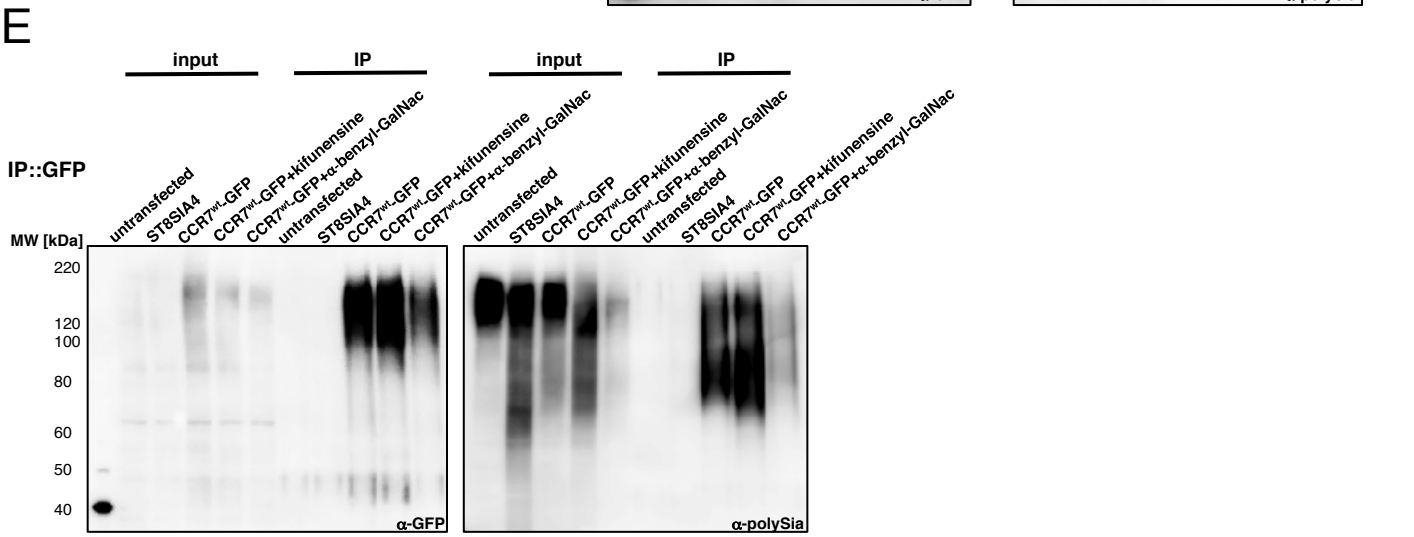

Figure S5

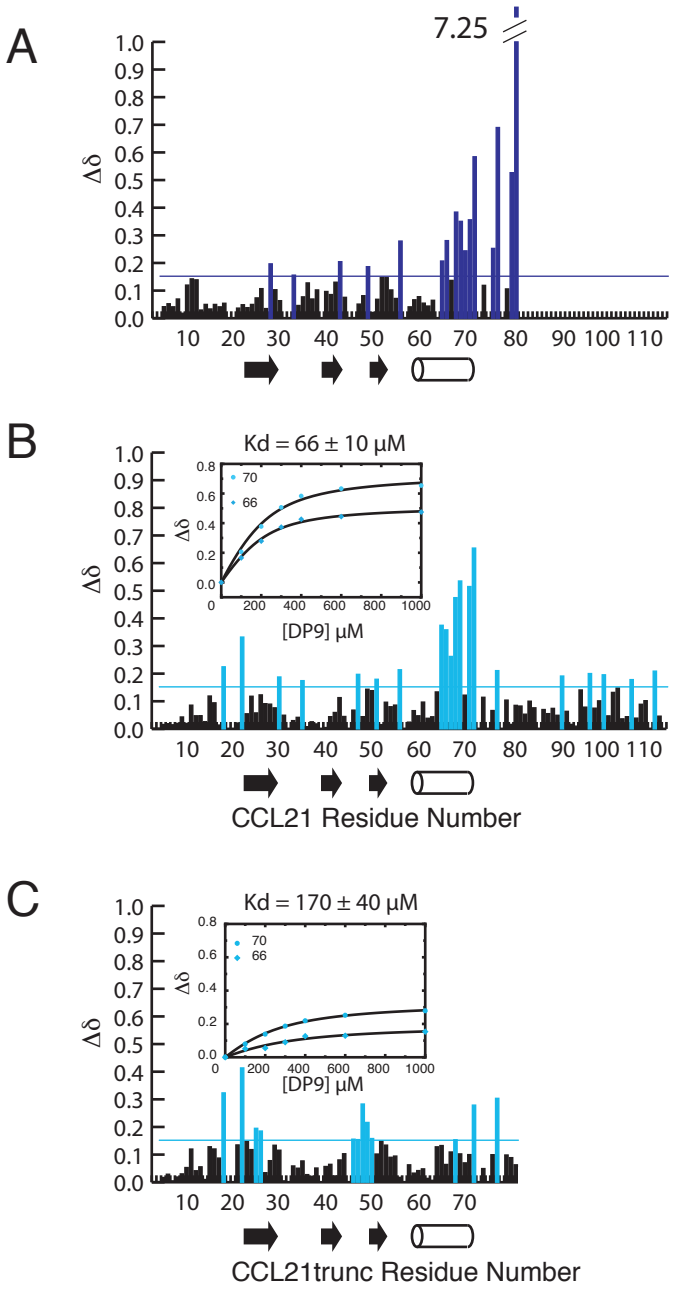
A
7.25
Δδ
1.0
0.9
0.8
0.7
0.6
0.5
0.4
0.3
0.2
0.1
0.0
10 20 30 40 50 60 70 80 90 100 110
B
Kd = 66 ± 10 μM
70
66
Δδ
0.8
0.6
0.4
0.2
0.0
0 200 400 600 800 1000
[DP9] μM
CCL21 Residue Number
C
Kd = 170 ± 40 μM
70
66
Δδ
[DP9] μM
10 20 30 40 50 60 70
CCL21trunc Residue Number